

SILAC Mouse for Quantitative Proteomics Uncovers Kindlin-3 as an Essential Factor for Red Blood Cell Function

Marcus Krüger,^{1,3} Markus Moser,^{2,3} Siegfried Ussar,² Ingo Thievensen,² Christian A. Luber,¹ Francesca Forner,¹ Sarah Schmidt,² Sara Zanivan,¹ Reinhard Fässler,^{2,*} and Matthias Mann^{1,*}

¹Department of Proteomics and Signal Transduction

²Department of Molecular Medicine

Max-Planck-Institute for Biochemistry, 82152 Martinsried, Germany

³These authors contributed equally to this work

*Correspondence: faessler@biochem.mpg.de (R.F.), mmann@biochem.mpg.de (M.M.)

DOI 10.1016/j.cell.2008.05.033

SUMMARY

Stable isotope labeling by amino acids in cell culture (SILAC) has become a versatile tool for quantitative, mass spectrometry (MS)-based proteomics. Here, we completely label mice with a diet containing either the natural or the ¹³C₆-substituted version of lysine. Mice were labeled over four generations with the heavy diet, and development, growth, and behavior were not affected. MS analysis of incorporation levels allowed for the determination of incorporation rates of proteins from blood cells and organs. The F2 generation was completely labeled in all organs tested. SILAC analysis from various organs lacking expression of β 1 integrin, β -Parvin, or the integrin tail-binding protein Kindlin-3 confirmed their absence and disclosed a structural defect of the red blood cell membrane skeleton in Kindlin-3-deficient erythrocytes. The SILAC-mouse approach is a versatile tool by which to quantitatively compare proteomes from knockout mice and thereby determine protein functions under complex in vivo conditions.

INTRODUCTION

The administration of radioactive or stable isotope tracers to animals is a well established technique by which to investigate the rate of protein synthesis and protein degradation. (Wolfe and Chinkes, 2005). This technology has been used for many decades (Schoenheimer and Rittenberg, 1935). The infusion of stable isotopes (¹³C or ¹⁵N) as tracers combined with measurements of ¹³CO₂ or ¹⁵N in urinary urea or ammonia is a broadly used technique by which to explore the amino acid flux in metabolic pathways (Bier, 1997; Dietz et al., 1982). Extensive incorporation of ¹³C or ¹⁵N stable isotopes does not result in discernable health effects of the treated animals (Doherty and Beynon, 2006; Gregg et al., 1973).

Mass spectrometry (MS) is not inherently quantitative, and relative protein expression changes are instead most accurately measured by comparison of the natural form of a peptide with its stable isotope analog (Ong and Mann, 2005). In recent years, ¹⁵N labeling has been applied to microorganisms such as yeast (Oda et al., 1999; Pratt et al., 2002), *Caenorhabditis elegans*, and *Drosophila* (Krijgsveld et al., 2003). Even a rat has been partially (Wu et al., 2004) or completely ¹⁵N labeled (McClatchy et al., 2007). In addition, nonsaturated labeling of a chicken, by using the essential amino acid valine, allows for the MS-based analysis of protein turnover rates in vivo (Doherty et al., 2005).

Our laboratory has previously described stable isotope labeling by amino acids in cell culture (SILAC) (Mann, 2006; Ong et al., 2002), which has unique advantages for quantitative and functional proteomics because of its inherent accuracy of quantitation and the ease of interpretation of MS results (Blagoev et al., 2004; Kratchmarova et al., 2005). In a SILAC experiment, two cell populations are generated: one in a medium that contains the natural amino acid (i.e., ¹²C₆-lysine), and the other in a medium that contains the heavy isotope-substituted version (i.e., ¹³C₆-lysine). This allows for direct comparison of protein expression levels by mixing the nonlabeled “light” and the labeled “heavy” cell populations (Cox and Mann, 2007). Each peptide appears as a pair in MS analysis with a difference in mass of 6 Da, and the relative peak intensities reflect the abundance ratios. To date, SILAC labeling has been limited to cell culture or microorganisms. To extend this powerful technique to higher organisms, Oda and coworkers have SILAC labeled the Neuro 2A cell line to serve as an internal standard for quantitation of a subset of peptides of the mouse brain proteome (Ishihama et al., 2005).

In the present paper, we report the development of a mouse SILAC diet that leads to complete labeling of the F2 generation. We used in vivo SILAC quantitation to analyze newly synthesized proteins from plasma and tissue samples in vivo. Furthermore, we validated our in vivo quantitation system by comparing the proteomes from platelets, heart, and erythrocytes from β 1 integrin-, β -Parvin-, and Kindlin-3-deficient mice, respectively.

Integrins are heterodimeric transmembrane proteins, consist of α and β subunits, are ubiquitously expressed, and perform

cell-cell and cell-matrix adhesion functions. Association of the corresponding α and β subunits is required for their stability and transport to the plasma membrane, as single subunits are not stable and are rapidly degraded. Integrin-mediated cell adhesion triggers intracellular signaling pathways (outside-in signaling) that control migration, proliferation, survival, and differentiation of cells. Prior to ligand binding, integrins require an energy-dependent activation step, which is triggered within the cell (inside-out signaling) and is characterized by a profound conformational change in both integrin subunits. Although the mechanism(s) underlying integrin activation are far from understood, it is believed that the binding of the FERM-domain-containing adaptor proteins talin and Kindlin to the integrin β cytoplasmic domains represents the last step in the activation pathway (Calderwood, 2004; Moser et al., 2008).

Upon activation and ligand binding, integrins recruit and assemble a multiprotein complex at the site of cell adhesion that fulfills two major tasks: it connects the extracellular matrix with the actin cytoskeleton, and it alters the fluxes of many intracellular signaling pathways. A preformed complex consisting of the three proteins, ILK, PINCH, and Parvin, represents an important component of the integrin adhesion complex (Legate et al., 2006). Parvins comprise a family of three proteins, α -, β - and γ -Parvin, that directly bind to ILK, F-actin, and other actin-associated proteins, thereby linking the adhesion complex to the actin cytoskeleton and controlling actin dynamics.

Kindlins have recently been identified within the integrin-mediated cell adhesion complex and represent an additional family of ILK-binding proteins (Montanez et al., 2007). They consist of three members (Kindlin-1–3) and are named after the gene mutated in Kindler syndrome, an autosomal recessive skin blister disease in humans. Kindlin-3 expression is restricted to hematopoietic cells, and the highest levels are in megakaryocytes (Ussar et al., 2006). Inactivation of the Kindlin-3 gene in mice results in severe anemia, which is thought to be due to a bleeding defect caused by impaired activation of platelet integrins, defects in platelet aggregation, and thrombus formation (Moser et al., 2008).

To screen for potential defects in other cellular compartments of the hematopoietic system in Kindlin-3-deficient mice, we compared their proteome with those from control mice. During the course of these studies, we discovered a deficit of structural proteins in the plasma membrane of Kindlin-3-deficient erythrocytes, which contributes to the severe anemia seen in Kindlin-3-deficient mice.

RESULTS

A Heavy SILAC Diet Has No Influence on Weight Gain and Fertility

We prepared a SILAC diet by mixing $^{13}\text{C}_6$ -lysine or $^{12}\text{C}_6$ -lysine into a customized lysine-free mouse diet to a final concentration of 1% (Figure 1A) according to standard mouse nutritional requirements (Benevenga et al., 1995). The amino acid content was subsequently checked by hydrolysis and cation exchange chromatography (Figure S1 available online). We first tested whether the diet permits normal weight gain by feeding mice with a regular diet or the SILAC diet (with $^{12}\text{C}_6$ -lysine or

$^{13}\text{C}_6$ -lysine). During an observation period of 4 weeks, all animals showed the same food consumption and a similar increase in body weight of about 17% (Figures S2A and S2B), normal fertility, and motor activity irrespective of the diet consumed. Furthermore, we SILAC labeled mice over four generations (see below), indicating that the labeling is compatible with normal development and physiology. Thus, we conclude that SILAC labeling with a $^{13}\text{C}_6$ -substituted essential amino acid diet does not lead to obvious discernable health effects in mice (Figure 1B).

SILAC Incorporation Rates Differ in Blood, Liver, and Gut Epithelium

To track $^{13}\text{C}_6$ -lysine incorporation into the proteome over time, we sampled blood each week for 4 weeks. Serum proteins were separated on 1D gels in triplicate, in-gel digested, and analyzed by high-resolution MS. The average relative standard deviation of all quantified proteins was $\sim 20\%$ (Figure 1C), an accuracy similar to what was seen in previous SILAC quantitation experiments (Blagoev et al., 2004; Ong et al., 2003).

As an example of different incorporation levels, SILAC peptide pairs of three serum proteins and one red blood cell protein are shown in Figure 1C. For serum albumin, we observed a SILAC ratio of 1:3.2, indicating that at least 74% of the protein had been newly synthesized during the first week of feeding. Because proteins can be synthesized from dietary amino acids as well as from amino acids derived by protein catabolism, this value is a lower limit for the true turnover (Beynon and Pratt, 2005). After 4 weeks, the three serum proteins were labeled to 90%. In contrast, hemoglobin was only labeled to 57% after 4 weeks (Figure 1C), due to the 60-day half-life of mouse erythrocytes (Berlin et al., 1959). Additional profiles of blood proteins are listed in Table S1.

Next, we measured the labeling efficiencies of a number of organs after 4 weeks of feeding with the SILAC diet. Proteins from heart showed an average protein ratio of 1:4.4 (Figure 2A; Table S2), much lower than the serum proteins. Furthermore, the distribution of SILAC ratios was relatively broad, reflecting the different incorporation rates of individual cell types and the “contamination” of serum proteins in nonperfused samples. For example, serum albumin has a similarly high incorporation rate in blood (ratio 9) and heart (ratio 10) (Figures 1C and 2A). In contrast to heart tissue, in which most cells are quiescent, the intestinal epithelium regenerates within a few days (Radtke and Clevers, 2005). Disaggregating the epithelium from the digestive tube resulted in a more homogeneous cell pool consisting of only a few cell types. As a consequence, we observed a high SILAC ratio of $1:9.1 \pm 2.1$ reflecting a labeling efficiency of more than 90% (Figure 2B), which is fully consistent with the high proliferation rate of this tissue. For example, villin-1, a marker for epithelial cells from the digestive system, showed a SILAC ratio of 1:10.

Liver has a number of different physiological roles, including carrying out metabolic functions and producing major blood proteins. Accordingly, we observed a wide distribution of SILAC-incorporation ratios among liver proteins. Hepatocytes are the predominant liver cell type, and they are very rich in mitochondria. To demonstrate that in vivo SILAC ratios can be measured with subcellular resolution, we isolated mitochondria from liver

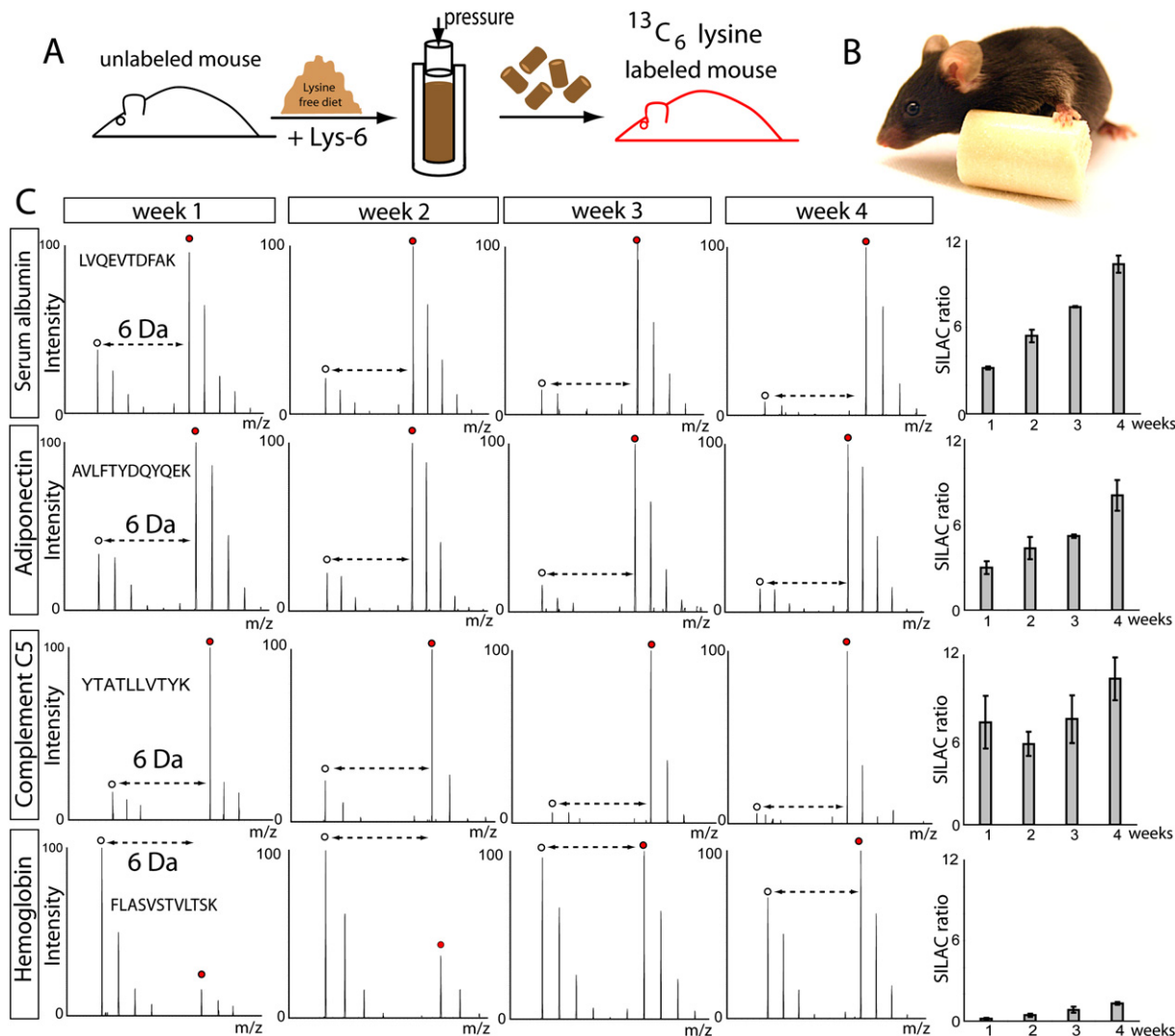


Figure 1. SILAC Labeling and Incorporation Rates of Blood Proteins

(A) Mice are SILAC labeled by being fed a pelleted, lysine-free diet supplemented with normal or heavy lysine.

(B) Mice on a SILAC diet cannot be visually distinguished from mice with a normal, commercial diet.

(C) Mass spectra showing SILAC pairs of a representative peptide for four blood proteins. The right-hand side shows lysine-6 incorporation over the course of 4 weeks as an average measurement of triplicates.

cells (Forner et al., 2006) and compared their labeling ratios to whole-cell lysates from the same sample (Figure 2C, black bars). Interestingly, proteins from mitochondria showed an average SILAC ratio of $1:8.6 \pm 2.4$. This shows that the incorporation rates of an organelle are more narrowly distributed and distinguishable from that of a whole tissue.

We next investigated several cell types of the hematopoietic system. Platelets are cell fragments that are constantly released by megakaryocytes into the blood stream. They have a half-life of ~7–9 days. We isolated platelets from a SILAC mouse after 4 weeks of labeling and measured incorporation levels of 86% from 241 quantified proteins (Figure 2D). In contrast, serum albumin, which was also measured within the platelet sample due to serum contamination, has a much higher incorporation level

compared to platelet proteins. Analysis of the red blood cell proteome revealed a significantly lower $^{13}\text{C}_6$ -lysine incorporation of 75% (Figure 2E). Thus, consideration of SILAC-incorporation rates could aid in the determination of the origin of the same proteins from different cellular pools via their different dynamic incorporation rates.

To combine SILAC-mouse analysis with cell sorting to obtain an accurately defined cell population, we separated CD45R-positive B lymphocytes from spleen by fluorescence-activated cell sorting (FACS) (Figures 2F and S3). An in-solution protein digest was performed from lysates of 1×10^6 spleen cells (Table S2F). The distribution of measured ratios was $1:5.4 \pm 1.3$, demonstrating that FACS-sorted populations of interest can readily be investigated in the SILAC mouse.

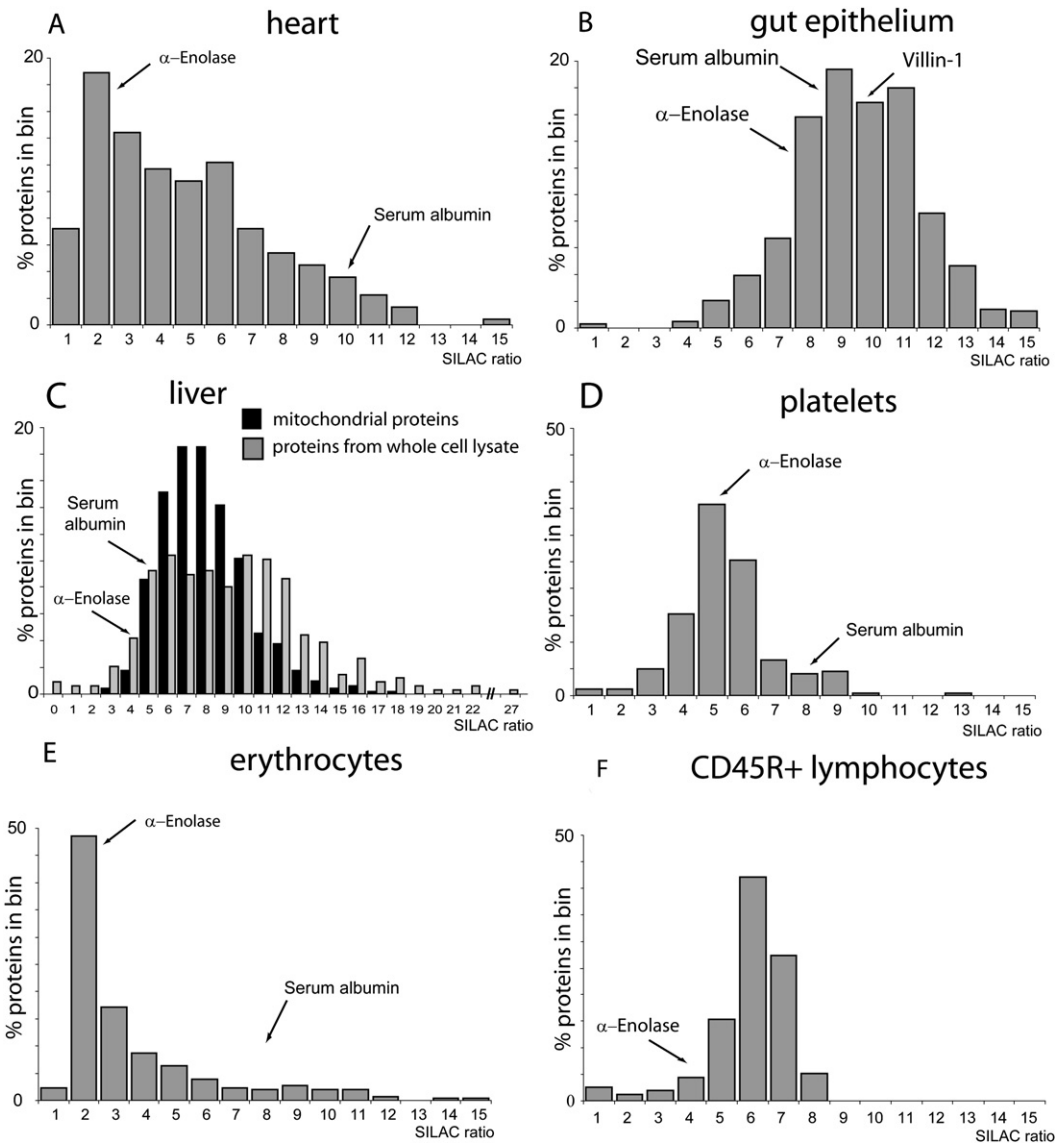


Figure 2. SILAC Label Incorporation into Different Cell Types and Tissues after 4 Weeks

(A–F) The panels show the relative number of proteins with the specified ratios for each proteome investigated. (A) Heart tissue. (B) Gut epithelium. (C) Incorporation into whole liver (gray bars) is compared with incorporation into liver mitochondria (black bars). (D) Platelets. (E) Erythrocytes. (F) CD45R-positive B lymphocytes from spleen.

Taken together, our results indicate that feeding mice with a SILAC diet is a suitable approach to label proteins *in vivo* and to follow their metabolic incorporation in any organ.

Complete SILAC-Based Labeling of F2 Mice

Although the label efficiency was relatively high in many tissues, we found that extending the labeling time did not lead to complete labeling. This is likely due to the recycling of internal amino acid sources (Doherty et al., 2005). Since labeling rates above 95% are required to perform comparative and quantitative proteomics by MS, we started feeding our mice over several generations with the heavy diet. Importantly, the consumption of the heavy diet did not affect litter size (Figure S2). The F1–F4 off-

spring developed normally, gained weight within the normal weight-gain chart (Figure S2), and showed normal mating behavior. Furthermore, newborn animals of the F1 generation were almost completely labeled, reaching ~93% in blood, brain, and liver (Figures 3 and S4). To obtain fully labeled animals to serve as internal standards and to investigate if SILAC labeling could be performed for many generations, we bred F2, F3, and F4 mice. These mice contained virtually no unlabeled peptides (Figures 3B, 3C, and 5A; Table S3).

Proteome of $\beta 1$ Integrin-Deficient Platelets

For validation of our *in vivo* quantitative proteomics approach, we analyzed and compared protein lysates from $\beta 1$ integrin-deficient

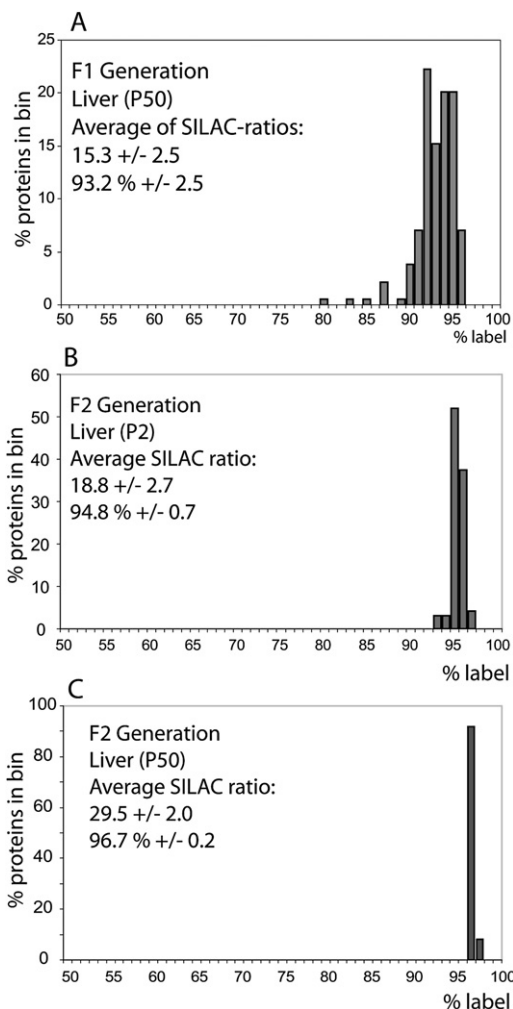


Figure 3. Complete Labeling of the F2 Generation

(A) Label efficiency of the liver of a 2-day-old mouse of the F1 generation. (B and C) Histograms of liver proteins with the specified percent incorporation at (B) P2 and at (C) P50 of the F2 generation. The averages of the SILAC ratios and the corresponding percent of the SILAC labeling are displayed in the histogram. The analysis encompasses ~100 proteins.

and control platelets (Nieswandt et al., 2001). We generated $\beta 1$ integrin-deficient platelets by intercrossing $\beta 1$ floxed mice ($\beta 1^{fl/fl}$) with a transgenic mouse expressing an Mx1 promoter-driven, interferon-inducible Cre (Mx1-Cre) (Brakebusch et al., 2000; Kuhn et al., 1995). We treated $\beta 1^{fl/fl}$; Mx1-Cre mice with synthetic double-stranded RNA (polyinosinic-polycytidylic acid, pl-pC), which triggers endogenous interferon production and subsequent Mx1-Cre activity. This leads to deletion of the $\beta 1$ integrin gene in all hematopoietic cells, including megakaryocytes. To monitor the knockout efficiency of $\beta 1$ integrin, we compared platelets from labeled wild-type animals with platelet populations from three groups of mice: (1) nonlabeled wild-type platelets; (2) platelets from nonlabeled, non-pl-pC-induced $\beta 1^{fl/fl}$; Mx1-Cre mice; and (3) platelets from nonlabeled, pl-pC-induced $\beta 1^{fl/fl}$; Mx1-Cre mice (Figure 4). All mice were backcrossed on a C57BL/6 background to reduce genetic variability.

We quantified ~645 proteins in these platelets, and, as expected, protein ratios of labeled and nonlabeled wild-type platelets were tightly distributed, with an overall ratio of 1:1. The quantitative MS analysis revealed complete loss of $\beta 1$ integrin in platelets from pl-pC-induced $\beta 1^{fl/fl}$; Mx1-Cre mice (Figure 4F). The proteins with the next highest ratios were the dimerization partners of the $\beta 1$ integrin subunit, strikingly confirming the sensitivity and reliability of our SILAC-mouse labeling system (Figure 4I). In a boxplot analysis, $\beta 1$, $\alpha 2$, and $\alpha 6$ integrins were all more than ten interquartile ranges away from the median (Figure S5A; Table S4). The complete loss of both α subunits can be explained by the formation of a stable integrin heterodimer during the synthesis and transport of the complexed integrin subunits to the plasma membrane. Without the correct β integrin subunit, the α subunit is rapidly degraded (Hynes, 2002). In contrast, the loss of $\beta 1$ integrin has no impact on the expression of other integrins, such as the major platelet integrin $\alpha IIb\beta 3$.

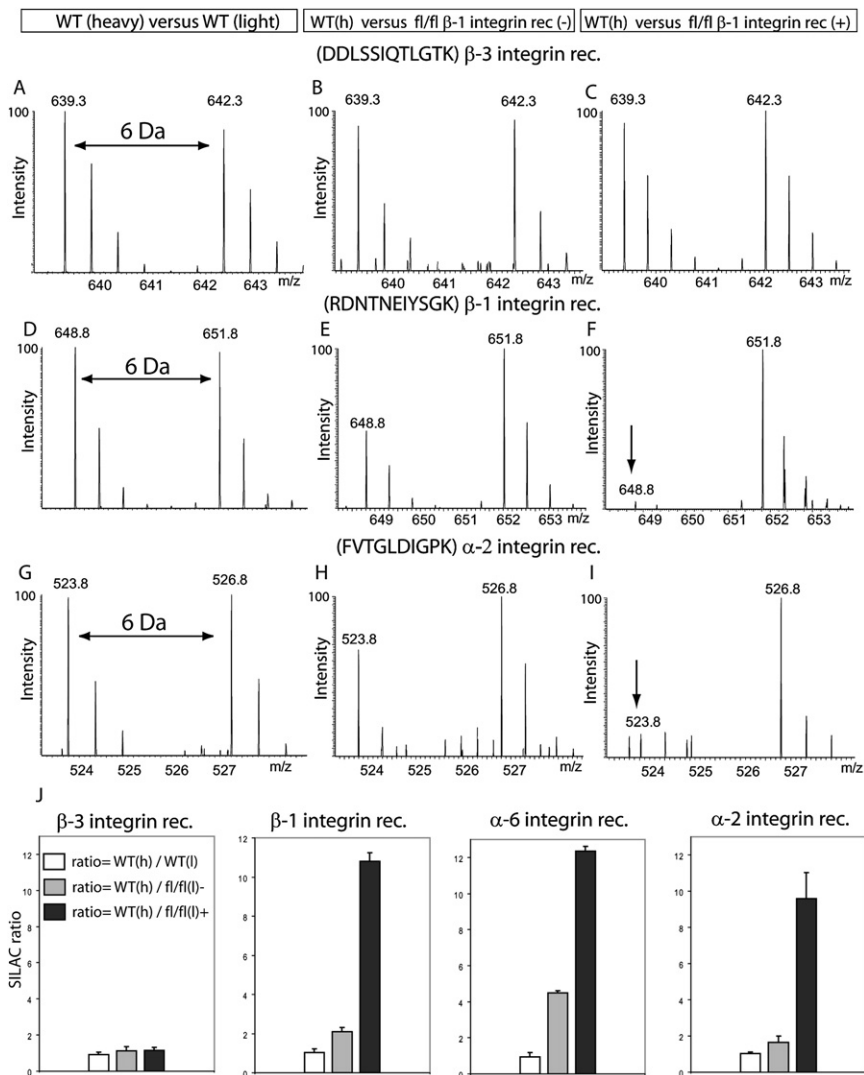
In addition, several other proteins in $\beta 1$ integrin-deficient platelets were outliers in the boxplot (Figure S5A; Table S4). However, a second independent experiment did not verify these proteins as being significantly downregulated. (Figure S5C). In contrast, the $\beta 1$ integrin dimerization partners $\alpha 2$ and $\alpha 6$ integrins were again strongly reduced (Figure S5).

Interestingly, the analysis of platelets from noninduced $\beta 1^{fl/fl}$; Mx1-Cre mice also revealed a slight downregulation of the $\beta 1$, $\alpha 2$, and $\alpha 6$ integrin levels compared to labeled wild-type platelets (Figure 4J). This effect is due to the natural, endogenous α/β interferon production in the bone marrow causing a low Mx1 promoter activity (Kuhn et al., 1995). The detection of this “leak” impressively underscores the sensitivity of our quantitative proteomics approach.

β -Parvin Deficiency in Heart Is Compensated by α -Parvin Induction

We next wanted to confirm the applicability of our in vivo SILAC approach to analyze the proteomes from knockout mice in a solid organ. To this end, we compared the proteomes from hearts of β -Parvin-deficient mice with those of control littermates. As a heavy standard, we used heart lysates from 2-week-old mice of the F4 generation, which showed an overall 97.7% incorporation of ^{13}C -lysine (Figure 5A). To test our quantitation system, we mixed “heavy” and “light” protein lysates from wild-type hearts in ratios of 1:1, 1:2, and 1:4. As shown in (Figure 5B), mixing of protein lysates from different heart samples gave rise to SILAC ratios that accurately reflected the lysate mixture.

β -Parvin represents the dominant Parvin isoform of the heart, since α -Parvin is only weakly present and γ -Parvin is absent from heart tissue. β -Parvin-deficient mice were generated by homologous recombination of a targeting vector in embryonic stem (ES) cells, which lacks exons 2 and 3 of the β -Parvin gene (I.T. and R.F., unpublished data). β -Parvin-deficient mice were viable and fertile and did not show any overt phenotype, indicating that β -Parvin is not essential for mouse development and organ formation. Mass spectrometric measurements of whole protein lysates from β -Parvin-deficient and control hearts of 2-week-old animals showed a complete absence of β -Parvin in knockout animals (Figures 5C and 5D). Out of 1205 proteins, only 4 proteins showed a two-fold decrease in their abundance compared to



wild-type hearts (Table S5). Interestingly, lack of β -Parvin had no dramatic consequence on the level of ILK and PINCH-1, which are the two other components of the ILK/Pinch/Parvin complex. The two-fold increase of α -Parvin in β -Parvin-deficient hearts suggests that the absence of an obvious phenotype is due to compensatory upregulation of α -Parvin (Figure 5C).

Kindlin-3 Deficiency Disrupts the Red Blood Cell Membrane Skeleton

Kindlin-3-deficient mice die at birth and suffer from severe bleeding, anemia, and pale skin color (Figures 7A and 7B; Moser et al., 2008). To further validate the power of *in vivo* SILAC and to obtain novel insights into Kindlin-3 function, we performed quantitative proteomics of platelets and erythrocytes from Kindlin-3^{-/-} mice. Platelet analysis identified Kindlin-3 as the protein with the highest fold change of more than 1200 platelet proteins (Figure S6A; Table S6). Interestingly, the levels of integrin α IIb and β 3 subunits were normal, suggesting that the reduced surface levels found by FACS (Moser et al., 2008) were due to an im-

Figure 4. Analysis of β 1 Integrin Knockout Platelets

(A–J) (A, D, and G) Platelets from SILAC-labeled wild-type mice were mixed with platelets from a nonlabeled wild-type control mouse. Comparison of the wild-type SILAC mouse with (B, E, and H) noninduced β 1^{fl/fl}; Mx1-Cre mice and with (C, F, and I) pl-pC-induced β 1^{fl/fl}; Mx1-Cre mice. The slight decrease of β 1 integrin shown in (E) is due to Cre activity induced by low endogenous interferon expression. The arrows in (F) and (I) label the reduced peak intensity of β 1 and α 2 integrin, respectively. (J) Summary of quantified SILAC ratios for β 3, β 1, α 2, and α 6 integrin subunits. White bars represent the ratio between the labeled wild-type WT(h) animal and the nonlabeled wild-type animal, gray bars represent the SILAC ratio of WT(h) and noninduced β 1^{fl/fl}, and black bars represent the SILAC ratio between WT(h) and induced β 1^{fl/fl}; Mx1-Cre. The error bars show the variability of the measured ratios.

paired integrin trafficking in the absence of Kindlin-3 (Figure S6B).

We have previously reported that Kindlin-3 (also known as “unc-related protein 2”) is present in red blood cells (Pasini et al., 2006). This was confirmed by different SILAC-incorporation levels in platelets (incorporation rate of 1:6.0) compared to erythrocytes (incorporation rate of 1:2.1), measured after the initial 4-week labeling period (Figures 2, S7A, and S7B). Furthermore, Kindlin-3 gene activity in Ter119-positive Kindlin-3-heterozygous erythroblasts was further corroborated by measuring Kindlin-3 promoter-driven β -galactosidase reporter gene activity with FACS (Figure S7C).

To investigate whether loss of Kindlin-3 affects erythroid cells, we determined and quantitatively compared the proteomes from wild-type, Kindlin-3^{+/-}, and Kindlin-3^{-/-} erythrocytes (Figure 6; Table S7). MS confirmed a 50% reduction of Kindlin-3 in heterozygous and a complete absence of Kindlin-3 in Kindlin-3^{-/-} erythrocytes (Figure 6A). Out of 881 proteins identified in all 3 proteomes, more than 50 were two-fold increased in Kindlin-3^{-/-} erythrocytes, and only a few revealed a more than two-fold reduction. Interestingly, a large proportion of the upregulated proteins was annotated to be nuclear (Table S7).

Blood smears from Kindlin-3^{-/-} embryos and P3 animals showed a strong reduction of cells when compared to wild-type controls and, in concordance with this proteomic finding, many more nucleated erythroblasts (Figures 7B and 7C). In addition, the size and shape of Kindlin-3^{-/-} erythrocytes were markedly irregular.

Scanning electron microscopy showed abnormally shaped erythrocytes with striking membrane invaginations and protuberances (Figure 7D). Red blood cell membrane abnormalities

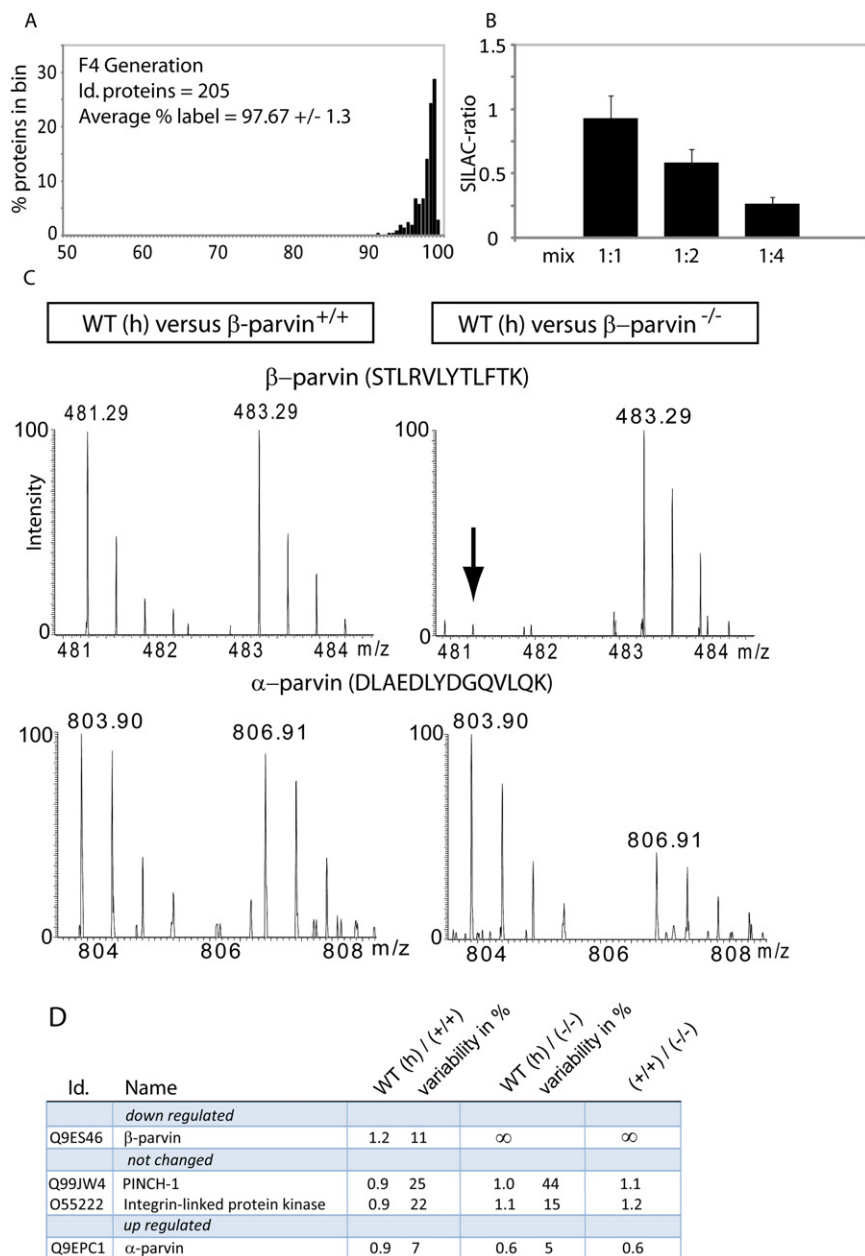


Figure 5. Analysis of Heart Tissue from β -Parvin Knockout Mice

(A) $^{13}\text{C}_6$ -Lysine incorporation of heart tissue from mice of the F4 generation shows a label efficiency of 97.7%.

(B) Heart tissue from labeled and nonlabeled animals was mixed 1:1, 1:2, and 1:4. The measured SILAC ratios after in-solution digestion were 0.93 ± 0.17 for the 1:1 mix, 0.58 ± 0.10 for the 1:2 mix, and 0.26 ± 0.05 for the 1:4 mix. Approximately 300 SILAC protein ratios were used for the quantification.

(C) Heart tissue from SILAC-labeled wild-type mice was mixed with nonlabeled β -Parvin (+/+) and β -Parvin (-/-) hearts. The arrow indicates the complete absence of β -Parvin.

(D) SILAC ratios of selected proteins.

and Kindlin-3^{-/-} mice and compared them to ghosts from SILAC-labeled control animals (Figure 7E). Quantitative SILAC-based analysis revealed an almost complete absence of ankyrin-1, band 4.1, adducin-2, and dematin (Figure 7F, right rows; Table S8), whereas other membrane-skeleton proteins, like α/β spectrin and band 3, were not changed.

Together, these findings show that Kindlin-3 is required for the assembly of a subset of proteins within the red blood cell membrane skeleton. Furthermore, the proteomic, morphological, and functional data provide a clear explanation for the anemia that leads to postnatal lethality.

DISCUSSION

Thus far, quantitative gene expression comparisons in higher organisms have been restricted to RNA analyses by gene chip approaches. These methods have many advantages: for example, ready accessibility and the fact that, in principle, almost all genes can be analyzed on one

are often caused by mutations within membrane-skeleton proteins, and the absence of key components can have drastic consequences on the stability of the red cell membrane (Delaunay, 1995). To obtain an explanation for the structural defects, we quantitatively compared the membrane-skeleton proteins from total erythrocytes by using SILAC-based MS. The levels of the most prominent skeleton proteins (e.g., α/β spectrin, ankyrin, band 3, band 4.1, band 4.2, and actin) did not significantly differ between wild-type and Kindlin-3^{-/-} mice.

Next, we determined whether these proteins have formed a stable meshwork that is connected with the erythrocyte membrane. To address this question, we isolated the erythrocyte membranes (so called red blood cell "ghosts") from wild-type

chip. However, because of posttranscriptional regulation as well as regulated protein degradation, these data do not necessarily predict changes in protein levels within cells or tissues. Furthermore, there are specific cell populations, such as the platelets and erythrocytes investigated here, that are devoid of mRNA and are therefore out of reach for these techniques.

Here, we show that SILAC, a versatile and successful method for quantitative proteomics in cell culture-based systems or microorganisms, can be extended to mammalian model systems. Mice can be SILAC labeled without any obvious effect on growth, behavior, or fertility. SILAC food preparation is straightforward and not particularly expensive when considering other resources required for the generation and maintenance of

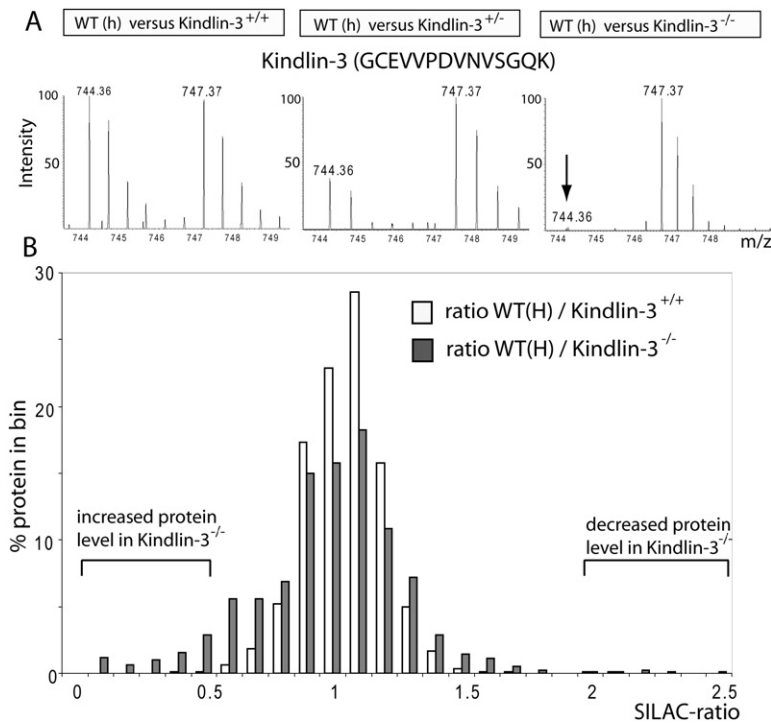


Figure 6. Quantitative Proteomics of Erythrocytes from Kindlin-3^{-/-} Mice

(A) Mass spectra of a Kindlin-3 peptide SILAC pair in Kindlin-3^{+/+}, Kindlin-3^{+/-}, and Kindlin-3^{-/-} erythrocytes. (B) Histogram of SILAC ratios of wild-type (white bars) and Kindlin-3^{-/-} (gray bars) erythrocytes. The measured ratios were grouped into ratio bins, and the y axis shows the relative number of detected ratios per bin.

knockout animals. We chose ¹³C₆-lysine labeling, as lysine is not converted into other amino acids. This makes endoprotease Lys-C the preferred choice as the proteolytic enzyme. Another interesting enzyme for SILAC mice is Lys-N, which has recently been described as an efficient enzyme for proteomics and de novo peptide sequencing (Taouatas et al., 2008). Organs derived from SILAC mice can serve as standards for a large number of subsequent experiments, in which wild-type and knockout mice are compared. Importantly, cell types such as intestinal epithelium that are difficult to study *ex vivo* can be analyzed by the *in vivo* SILAC approach. Moreover, the SILAC mouse can serve as a reference model at any biological scale, from the whole organ through specific cell types down to intracellular compartments or single proteins of interest. As an example, we used SILAC mice to successfully study the mitochondrial proteome, which can be extended to investigations in relevant organs from metabolic or neurodegenerative disease models. In studies in which a large number of mice are required—such as in toxicology studies—labeled organ tissue could be stored and used as an internal standard for each measurement. A labeled SILAC-mouse liver, for example, yields sufficient internal standard for more than 1000 measurements. Although not shown here, phosphopeptides can also be enriched from SILAC mice and can serve as a standard for functional and time-resolved phosphoproteomics (Olsen et al., 2006).

We analyzed the proteomes of cells from three independent knockout mice. In all analyses, the complete absence of the targeted genes was immediately revealed by the SILAC technique. Furthermore, heterozygous Kindlin-3 animals present the expected two-fold reduction from wild-type levels, emphasizing the quantitative nature of our proteomic technology. This may be particularly useful in quantifying knockdown efficiencies in

transgenic RNAi mice. The sensitivity of the SILAC-based quantitation system became remarkably obvious by an observation from the β 1 integrin inactivation in platelets. Deletion of the β 1 integrin gene in hematopoietic cells is achieved by the induction of the Mx1-Cre transgene through the injection of pI-pC into β 1 integrin floxed animals. Even without induction of Cre, the low expression levels of naturally expressed α/β interferon activated the Mx1 promoter and triggered β 1 integrin deletion in a few cells. Even this slight difference in total β 1 integrin expression proved sufficient for detection by the SILAC method.

Our proteomic data on platelets of β 1 integrin mice showed that, although integrins control a number of different signaling pathways, the lack of the

β 1 integrin has no consequences on the levels of other proteins in platelets, apart from its dimerization partners α 2 and α 6 integrins. This may be due to the fact that, in resting platelets, integrins are inactive and signaling into the cell is only induced upon stimulation via molecules like thrombin or collagen (Ruggeri, 2002). Further studies with the SILAC-mouse system could focus on activation of signaling cascades during platelet aggregation by using phosphoproteomics.

To test the SILAC-based analysis in a solid organ system, we compared the proteomes from heart of β -Parvin-deficient mice with control littermates. The complexity of a tissue, formed by different cell types, poses no limitation for the quantitative analysis by MS. The interpretation of results, however, is more challenging because changes in protein levels may result from non-cell-autonomous defects caused, for example, by altered cell-cell communication rather than cell-autonomous defects.

To study the molecular cause of the anemia observed in Kindlin-3 mutants, we analyzed the consequences of this deletion on the proteome of platelets and erythrocytes. Recently, we characterized Kindlin-3 as an essential factor for the activation of platelet integrins (Moser et al., 2008). Kindlin-3 directly binds to the cytoplasmic tails of both β 1 and β 3 integrin subunits. Its expression is restricted to cells of the hematopoietic system (Ussar et al., 2006). Our SILAC-based analysis of Kindlin-3-deficient erythrocytes revealed an increased amount of nuclear proteins, prompting us to investigate consequences of the knockout on this cell type. Consistent with the proteomic results, we found an increased number of nucleated erythroblasts in blood smears. Furthermore, Kindlin-3-deficient erythrocytes are irregular in size and shape. The structural defects of the red blood cell membrane skeleton suggested an additional function of Kindlin-3. With the help of the SILAC method, we quantitatively

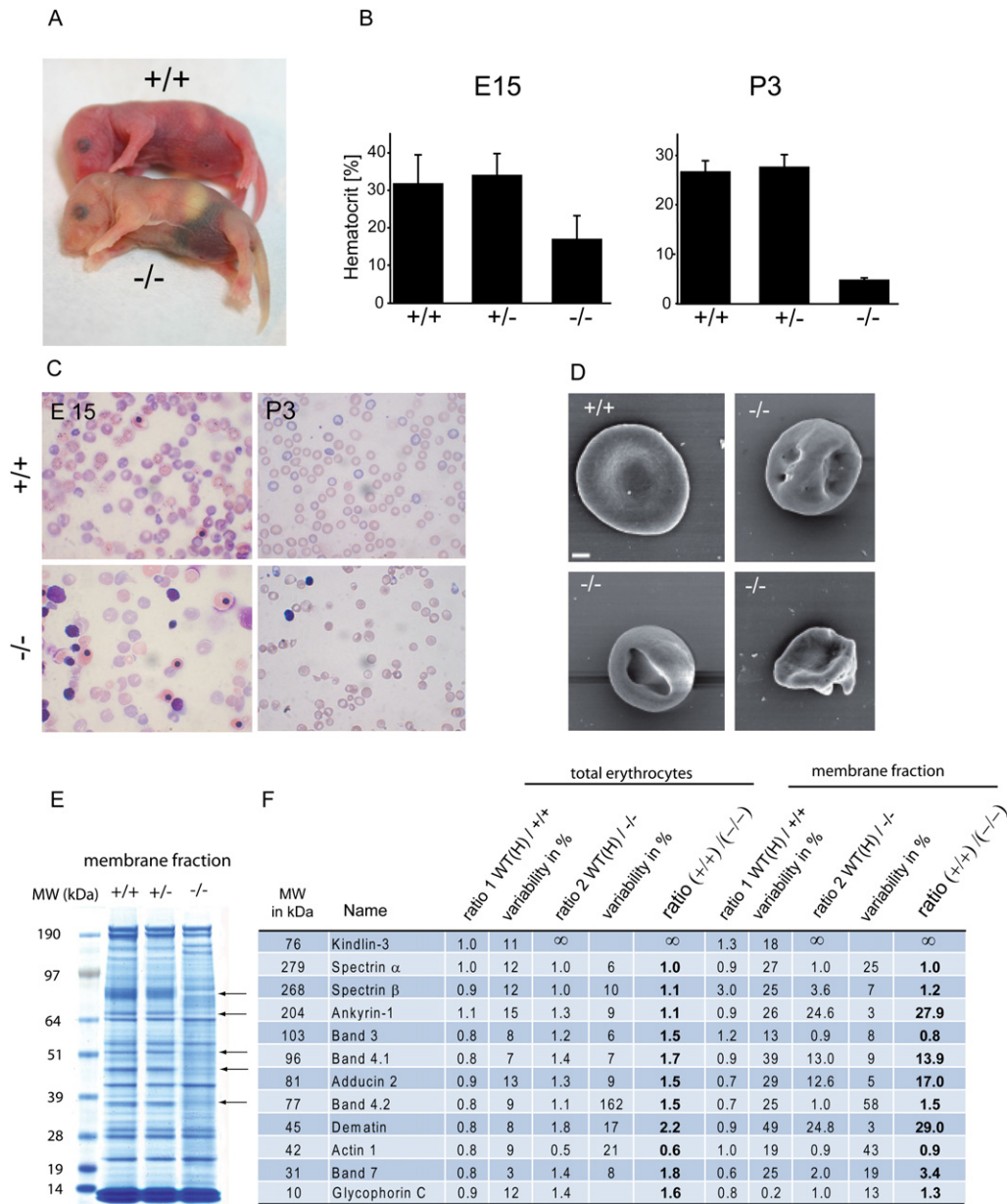


Figure 7. Kindlin-3-Deficient Erythrocytes Show Disrupted Membrane Skeletons

- (A) Kindlin-3 knockout mice are anemic.
 (B) Decreased hematocrit in Kindlin-3^{-/-} mutants at embryonic day 15 and P3.
 (C) Blood smears from E15 embryos and P3 wild-type and Kindlin-3^{-/-} mice reveal fewer erythrocytes and an increased number of nucleated erythroblasts.
 (D) Scanning electron microscopy of wild-type and Kindlin-3^{-/-} erythrocytes. The scale bar represents 1 μ m.
 (E) "Ghost" lysates from wild-type, heterozygous, and Kindlin-3^{-/-} mice were stained by Coomassie blue after SDS-PAGE. The arrows indicate the absence of proteins within the membrane-skeleton fraction of Kindlin-3^{-/-} erythrocytes.
 (F) SILAC-ratio comparison of total erythrocytes (left rows) and the membrane fraction (right row).

compared the membrane-skeleton proteins of control and Kindlin-3-deficient erythrocytes and revealed a critical role of Kindlin-3 in the formation or stabilization of this structure. The inner surface of the red blood cell membrane is laminated by a protein network that is linked to transmembrane proteins. In humans and mice, mutations in genes encoding ankyrin, band 3, spec-

trin, and protein 4.1 or protein 4.2 cause hereditary spherocytosis or poikilocytosis, often accompanied with hemolytic anemias (DeLaunay, 1995; Peters et al., 1998; Rybicki et al., 1995; Shi et al., 1999; Southgate et al., 1996). The dramatic reduction of ankyrin-1, protein 4.1, and dematin in membrane preparations from Kindlin-3-deficient erythrocytes explains the severe

malformations. Thus, loss of Kindlin-3 affects erythropoiesis by disrupting the assembly of structural components within the red blood cell membrane skeleton.

In summary, a direct combination of the SILAC technology for quantitative proteomics with the large number of powerful mouse models generated by the community is now possible. We have demonstrated here how proteomics can be combined with several of the powerful technologies already used in this endeavor. We are confident that this technology will help to elucidate disease processes and guide novel intervention strategies.

Data Availability

Data used for quantitation accompany this article online.

EXPERIMENTAL PROCEDURES

Materials and Reagents

$^{13}\text{C}_6$ -Lysine (98 atom % ^{13}C) was purchased from Silantes, Martinsried, Germany. Chemicals for the “in-solution” and “in-gel” digests were purchased from Sigma-Aldrich, and LysC was obtained from WAKO. Wild-type mice were obtained from an in-house C57Bl/6 colony.

Knockout Mice

Transgenic mice expressing the Cre recombinase under the control of the Mx1 promoter (Kuhn et al., 1995) were mated with mice carrying a floxed $\beta 1$ integrin gene (Brakebusch et al., 2000). To ensure extensive downregulation of the $\beta 1$ integrin on platelets, pl-pC (250 μg per mouse) (Amersham) was injected intraperitoneally three times in a 2-day interval.

Kindlin-3-deficient mice were generated as described by Moser et al. (2008). A detailed description of the β -Parvin gene inactivation will be published elsewhere (I.T. and R.F., unpublished data).

Food Preparation, Weight Gain, and Food Consumption

A customized lysine-free mouse diet (Harlan-Teklad, TD.99386) was combined with the heavy $\text{L-}^{13}\text{C}_6$ -lysine and the natural isotope L- lysine (Sigma) to a final concentration of 1%. To obtain a homogenous distribution of the amino acid, the powder was vigorously mixed with a blender for 5 min. For the preparation of food pellets, ~ 10 g of the mixture was filled into an in-house-manufactured cylinder with an inner diameter of 1.5 cm and a length of 10 cm. Food was compressed with an exactly fitting pestle for 1 min. Pellets were taken out and dried overnight at room temperature. After drying, the pellets were cut into smaller pieces.

The lysine content was checked as described (Moore et al., 1958). Although the hydrolysis with subsequent chromatography does not allow for the exact determination of the amino acid contents, the supplemented lysine amount was comparable to that in the customized diet containing the natural lysine isotope.

For testing weight gain and food consumption, one group ($n = 3$ females) was fed with a regular mouse diet, one group ($n = 3$ females) was fed with the customized lysine-free diet supplemented with natural lysine (Sigma), and one animal was fed with the diet containing the heavy isotope for lysine. All animals were fed ad libitum and had access to water.

Food consumption was measured daily for 10 days during breeding and weaning periods (Figure S2). The label percentage was calculated as the mean of the heavy-labeled peptide signal divided by the sum of the light and heavy signals.

Sample Preparation

Blood Samples

Mice were anesthetized with isofluran, and 20 μl blood was taken from the retro-orbital plexus. Blood samples were incubated with heparin (20 U/ml), and, after centrifugation, the supernatant was frozen in liquid nitrogen and stored at -80°C .

Tissue Harvest

After sacrificing animals by cervical dislocation, tissues were dissected, washed in phosphate-buffered saline (PBS [pH 7.4]), and frozen in liquid nitrogen. For protein isolation, tissues were homogenized in a buffer containing 1% NP-40, 0.1% sodium deoxycholate, 150 mM NaCl, 1 mM EDTA, 50 mM Tris (pH 7.5), and protease inhibitors (Complete tablets, Roche). The lysates were centrifuged at $14,000 \times g$ to pellet cellular debris. A Bradford assay was performed to determine protein concentrations of the supernatants.

Mitochondria Isolation

Liver tissue was quickly washed in water, then washed three times in 250 mM sucrose, 10 mM Tris-HCl, 0.1 mM EGTA (pH 7.4) supplemented with protease inhibitors (Roche). Crude mitochondria were isolated as described previously (Forner et al., 2006) and were purified on a 30% Percoll density centrifugation gradient.

Platelets were isolated by differential centrifugation steps as described by Moebius et al. (2005).

Epithelial Cell Isolation from Gut

Small intestine was cut open and washed with PBS. The small intestine was transferred to dissociation buffer (130 mM NaCl, 10 mM EDTA, 10 mM HEPES [pH 7.4], 10% FCS, and 1 mM DTT) and was incubated for 45 min on a rotor at 37°C . The rest of the intestine was removed, and the epithelial clumps were collected by centrifugation at 800 rpm for 5 min and washed in PBS.

B Cell Isolation

For B cell isolation, spleen was cut into small fragments and digested with collagenase and DNase, followed by the addition of EDTA. Subsequently, cells were incubated with anti-CD45R, anti-CD3, and anti-CD49b (BD Pharmingen). B cells were selected as cells that stained positive for CD45R (B220) (Coffman, 1982) and negative for both anti-CD3 and anti-CD49b and were then sorted by using a FACS Aria system (Becton Dickinson).

Mass Spectrometry

For protein separation, samples were loaded on a NuPAGE 4%–12% Bis-Tris gel (Invitrogen). After staining of the gel with the Colloidal Blue Staining Kit (Invitrogen), evenly sized gel pieces were excised from the gel and processed for enhanced liquid chromatography-mass spectrometry (GelC-MS).

For blood analysis, Coomassie-stained gel lanes were cut into eight pieces. To determine incorporation ratios, we analyzed three gel pieces per lane from heart, gut epithelia, liver, red blood cell, and platelet samples.

The gel pieces were subjected to in-gel reduction and alkylation, followed by LysC digestion as previously described (Andersen et al., 2005; Shevchenko et al., 1996). Finally, peptides were extracted twice by adding an equal volume of 30% acetonitrile/0.3% trifluoroacetic acid (TFA) in water to digest the mixture, followed by a final extraction with 100% acetonitrile. Extracts were evaporated in a speedvac to remove acetonitrile and were subsequently acidified with 0.5% TFA. Samples were desalted and concentrated with StageTips and were resuspended in 5 μl of 0.5% acetic acid/1% TFA (Rappsilber et al., 2003). In-solution digestion of proteins was performed as described by Ong and Mann (2006).

Reverse-phase nano-LC-MS/MS was performed by using an Agilent 1100/1200 nanoflow LC system (Agilent Technologies) with a cooled, thermostated 96-well autosampler. The LC system was coupled to a 7-Tesla LTQ-FT or LTQ Orbitrap instrument (Thermo Fisher Scientific) equipped with a nano-electrospray source (Proxeon). Chromatographic separation of peptides was performed in a 10 cm long 8 μm tip opening/75 μm inner diameter capillary needle (Proxeon). The column was custom made with methanol slurry of reverse-phase ReproSil-Pur C18-AQ 3 μm resin (Dr. Maisch, GmbH). The LysC-digested peptide mixtures were autosampled at a flow rate of 0.5 $\mu\text{l}/\text{min}$ and then eluted with a linear gradient at a flow rate of 0.25 $\mu\text{l}/\text{min}$. The mass spectrometers were operated in the data-dependent mode to automatically measure MS and MS/MS. LTQ-FT full scan MS spectra (from m/z 300 to m/z 1600) were acquired with a resolution of $R = 100,000$ at m/z 400 (after accumulation to a target value of 3,000,000 in the linear ion trap). The five most intense ions were sequentially isolated and fragmented in the linear ion trap by using collisionally induced dissociation at a target value of 10,000 (Olsen et al., 2004).

Raw data files were converted to Mascot generic format files with in-house software (Raw2MSM), and Mascot (version 2.0) was used for a database search and protein identification. The following search

parameters were used in all MASCOT searches: LysC digest; no missed cleavage; carbamidomethylation of cysteine set as a fixed modification; and oxidation of methionines and L-lysine-6 allowed as variable modifications. The maximum allowed mass deviation for MS and MS/MS scans was 10 ppm and 0.5 Da, respectively. Only proteins that had at least two peptides with ion scores >20 were considered for identification and quantitation. MSQuant (Schulze and Mann, 2004) was used to verify and quantify the resulting SILAC-peptide pairs. All proteomic results were deposited in the publicly accessible MAPU database (Zhang et al., 2007). A target decoy database approach was used to identify false-positive peptides and to set threshold criteria such that <1% false positives were included in the peptide list (Tables S1 and S2, statistics sheet). After mass recalibration with MSQuant, the average absolute mass error of all peptides was better than 3 ppm.

Samples from all mouse mutants were analyzed by the in-house-developed software MaxQuant (Cox and Mann, 2007; Graumann et al., 2008). Briefly, MaxQuant performs a peak list, SILAC- and XIC-based quantitation, false-positive rates (Gingras et al., 2007), and peptide identification based on Mascot search results.

All data were searched against the International Protein Index sequence database (mouse IPI, version 3.24) (Kersey et al., 2004). Fold-change for ghost proteins was determined from the gel slice corresponding to the expected migration of the full-length protein.

Blood Cell Analyses

Hematocrit was measured from peripheral blood with a hematology analyzer (Nihon Kohden).

For "ghost" preparation, erythrocytes were washed twice in 0.9% NaCl, 10 mM sodium phosphate buffer (pH 7.0) before hypotonic lysis were performed in 0.25% NaCl, 10 mM sodium phosphate buffer (pH 7.0). Lysis was performed in several rounds in hypotonic buffer until the pellet became white.

Flow Cytometry

Flow cytometric lacZ staining of hematopoietic cells was performed on Ter119-positive bone marrow cells that have been incubated with the fluorescent β -galactosidase substrate FDG (fluorescein di- β -D-galactopyranoside) (Sigma) as described (Montanez et al., 2007). Flow cytometry was carried out on a Becton Dickinson FACSCalibur.

SUPPLEMENTAL DATA

Supplemental Data include seven figures and eight tables for protein identification and quantification and are available with this article online at <http://www.cell.com/cgi/content/full/134/2/353/DC1/>.

ACKNOWLEDGMENTS

We thank other members of the department for proteomics and signal transduction and the Department of Molecular Medicine for sharing insights. Meredith O'Keeffe provided critical help in FACS sorting. We thank Gerhard Wanner for imaging erythrocytes by scanning electron microscopy. This work was supported by a long-term European Molecular Biology Organization fellowship to M.K., by the 6th and 7th framework program of the European Union, by the Austrian Science Foundation (SFB021), and by the Max Planck Society.

Received: February 18, 2008

Revised: April 29, 2008

Accepted: May 20, 2008

Published: July 24, 2008

REFERENCES

Andersen, J.S., Lam, Y.W., Leung, A.K., Ong, S.E., Lyon, C.E., Lamond, A.I., and Mann, M. (2005). Nucleolar proteome dynamics. *Nature* 433, 77–83.

Benevenga, N.J., Calvert, C., Eckhart, C.D., Fahey, G.C., Greger, J.L., Keen, C.L., Knapka, J.J., Magalhaes, H., and Oftedal, O.T. (1995). Nutrient require-

ments of the mouse. In *Nutrient Requirements of Laboratory Animals*, J. Overton, ed. (Washington, D.C.: National Academy Press), pp. 192.

Berlin, N.I., Waldmann, T.A., and Weissman, S.M. (1959). Life span of red blood cell. *Physiol. Rev.* 39, 577–616.

Beynon, R.J., and Pratt, J.M. (2005). Metabolic labeling of proteins for proteomics. *Mol. Cell. Proteomics* 4, 857–872.

Bier, D.M. (1997). Stable isotopes in biosciences, their measurement and models for amino acid metabolism. *Eur. J. Pediatr.* 156 (Suppl 1), S2–S8.

Blagoev, B., Ong, S.E., Kratchmarova, I., and Mann, M. (2004). Temporal analysis of phosphotyrosine-dependent signaling networks by quantitative proteomics. *Nat. Biotechnol.* 22, 1139–1145.

Brakebusch, C., Grose, R., Quondamatteo, F., Ramirez, A., Jorcano, J.L., Pirro, A., Svensson, M., Herken, R., Sasaki, T., Timpl, R., et al. (2000). Skin and hair follicle integrity is crucially dependent on β 1 integrin expression on keratinocytes. *EMBO J.* 19, 3990–4003.

Calderwood, D.A. (2004). Integrin activation. *J. Cell Sci.* 117, 657–666.

Coffman, R.L. (1982). Surface antigen expression and immunoglobulin gene rearrangement during mouse pre-B cell development. *Immunol. Rev.* 69, 5–23.

Cox, J., and Mann, M. (2007). Is proteomics the new genomics? *Cell* 130, 395–398.

Delaunay, J. (1995). Genetic disorders of the red cell membranes. *FEBS Lett.* 369, 34–37.

Dietz, W.H., Jr., Wolfe, M.H., and Wolfe, R.R. (1982). A method for the rapid determination of protein turnover. *Metabolism* 31, 749–754.

Doherty, M.K., and Beynon, R.J. (2006). Protein turnover on the scale of the proteome. *Expert Rev. Proteomics* 3, 97–110.

Doherty, M.K., Whitehead, C., McCormack, H., Gaskell, S.J., and Beynon, R.J. (2005). Proteome dynamics in complex organisms: using stable isotopes to monitor individual protein turnover rates. *Proteomics* 5, 522–533.

Forner, F., Foster, L.J., Campanaro, S., Valle, G., and Mann, M. (2006). Quantitative proteomic comparison of rat mitochondria from muscle, heart, and liver. *Mol. Cell. Proteomics* 5, 608–619.

Gingras, A.C., Gstaiger, M., Raught, B., and Aebersold, R. (2007). Analysis of protein complexes using mass spectrometry. *Nat. Rev. Mol. Cell Biol.* 8, 645–654.

Graumann, J., Hubner, N.C., Kim, J.B., Ko, K., Moser, M., Kumar, C., Cox, J., Schoeler, H., and Mann, M. (2008). SILAC-labeling and proteome quantitation of mouse embryonic stem cells to a depth of 5111 proteins. *Mol. Cell. Proteomics* 7, 672–683. Published online November 28, 2007. 10.1074/mcp.M700460-MCP200.

Gregg, C.T., Hutson, J.Y., Prine, J.R., Ott, D.G., and Furchner, J.E. (1973). Substantial replacement of mammalian body carbon with carbon-13. *Life Sci.* 13, 775–782.

Hynes, R.O. (2002). Integrins: bidirectional, allosteric signaling machines. *Cell* 110, 673–687.

Ishihama, Y., Sato, T., Tabata, T., Miyamoto, N., Sagane, K., Nagasu, T., and Oda, Y. (2005). Quantitative mouse brain proteomics using culture-derived isotope tags as internal standards. *Nat. Biotechnol.* 23, 617–621.

Kersey, P.J., Duarte, J., Williams, A., Karavidopoulou, Y., Birney, E., and Apweiler, R. (2004). The International Protein Index: an integrated database for proteomics experiments. *Proteomics* 4, 1985–1988.

Kratchmarova, I., Blagoev, B., Haack-Sorensen, M., Kassem, M., and Mann, M. (2005). Mechanism of divergent growth factor effects in mesenchymal stem cell differentiation. *Science* 308, 1472–1477.

Krijgsveld, J., Ketting, R.F., Mahmoudi, T., Johansen, J., Artal-Sanz, M., Verrijzer, C.P., Plasterk, R.H., and Heck, A.J. (2003). Metabolic labeling of *C. elegans* and *D. melanogaster* for quantitative proteomics. *Nat. Biotechnol.* 21, 927–931.

Kuhn, R., Schwenk, F., Aguet, M., and Rajewsky, K. (1995). Inducible gene targeting in mice. *Science* 269, 1427–1429.

Legate, K.R., Montanez, E., Kudlacek, O., and Fassler, R. (2006). ILK, PINCH and parvin: the tIPP of integrin signalling. *Nat. Rev. Mol. Cell Biol.* 7, 20–31.

- Mann, M. (2006). Functional and quantitative proteomics using SILAC. *Nat. Rev. Mol. Cell Biol.* 7, 952–958.
- McClatchy, D.B., Dong, M.Q., Wu, C.C., Venable, J.D., and Yates, J.R., 3rd. (2007). ¹⁵N metabolic labeling of mammalian tissue with slow protein turnover. *J. Proteome Res.* 6, 2005–2010.
- Moebius, J., Zahedi, R.P., Lewandrowski, U., Berger, C., Walter, U., and Sickmann, A. (2005). The human platelet membrane proteome reveals several new potential membrane proteins. *Mol. Cell. Proteomics* 4, 1754–1761.
- Montanez, E., Piwko-Czuchra, A., Bauer, M., Li, S., Yurchenco, P., and Fassler, R. (2007). Analysis of integrin functions in peri-implantation embryos, hematopoietic system, and skin. *Methods Enzymol.* 426, 239–289.
- Moore, S., Spackman, D.H., and Stein, W.H. (1958). Automatic recording apparatus for use in the chromatography of amino acids. *Fed. Proc.* 17, 1107–1115.
- Moser, M., Nieswandt, B., Ussar, S., Pozgajova, M., and Fässler, R. (2008). Kindlin-3 is essential for integrin activation and platelet aggregation. *Nat. Med.* 14, 325–330. Published online February 17, 2008. 10.1038/nm1722.
- Nieswandt, B., Brakebusch, C., Bergmeier, W., Schulte, V., Bouvard, D., Mokhtari-Nejad, R., Lindhout, T., Heemskerk, J.W., Zirngibl, H., and Fassler, R. (2001). Glycoprotein VI but not $\alpha 2\beta 1$ integrin is essential for platelet interaction with collagen. *EMBO J.* 20, 2120–2130.
- Oda, Y., Huang, K., Cross, F.R., Cowburn, D., and Chait, B.T. (1999). Accurate quantitation of protein expression and site-specific phosphorylation. *Proc. Natl. Acad. Sci. USA* 96, 6591–6596.
- Olsen, J.V., Ong, S.E., and Mann, M. (2004). Trypsin cleaves exclusively C-terminal to arginine and lysine residues. *Mol. Cell. Proteomics* 3, 608–614.
- Olsen, J.V., Blagoev, B., Gnäd, F., Macek, B., Kumar, C., Mortensen, P., and Mann, M. (2006). Global, in vivo, and site-specific phosphorylation dynamics in signaling networks. *Cell* 127, 635–648.
- Ong, S.E., and Mann, M. (2005). Mass spectrometry-based proteomics turns quantitative. *Nat. Chem. Biol.* 1, 252–262.
- Ong, S.E., and Mann, M. (2006). A practical recipe for stable isotope labeling by amino acids in cell culture (SILAC). *Nat. Protoc.* 1, 2650–2660.
- Ong, S.E., Blagoev, B., Kratchmarova, I., Kristensen, D.B., Steen, H., Pandey, A., and Mann, M. (2002). Stable isotope labeling by amino acids in cell culture, SILAC, as a simple and accurate approach to expression proteomics. *Mol. Cell. Proteomics* 1, 376–386.
- Ong, S.E., Kratchmarova, I., and Mann, M. (2003). Properties of ¹³C-substituted arginine in stable isotope labeling by amino acids in cell culture (SILAC). *J. Proteome Res.* 2, 173–181.
- Pasini, E.M., Kirkegaard, M., Mortensen, P., Lutz, H.U., Thomas, A.W., and Mann, M. (2006). In-depth analysis of the membrane and cytosolic proteome of red blood cells. *Blood* 108, 791–801.
- Peters, L.L., Weier, H.U., Walensky, L.D., Snyder, S.H., Parra, M., Mohandas, N., and Conboy, J.G. (1998). Four paralogous protein 4.1 genes map to distinct chromosomes in mouse and human. *Genomics* 54, 348–350.
- Pratt, J.M., Robertson, D.H., Gaskell, S.J., Riba-Garcia, I., Hubbard, S.J., Sidhu, K., Oliver, S.G., Butler, P., Hayes, A., Petty, J., et al. (2002). Stable isotope labelling in vivo as an aid to protein identification in peptide mass fingerprinting. *Proteomics* 2, 157–163.
- Radtke, F., and Clevers, H. (2005). Self-renewal and cancer of the gut: two sides of a coin. *Science* 307, 1904–1909.
- Rappsilber, J., Ishihama, Y., and Mann, M. (2003). Stop and go extraction tips for matrix-assisted laser desorption/ionization, nanoelectrospray, and LC/MS sample pretreatment in proteomics. *Anal. Chem.* 75, 663–670.
- Ruggeri, Z.M. (2002). Platelets in atherothrombosis. *Nat. Med.* 8, 1227–1234.
- Rybicki, A.C., Musto, S., and Schwartz, R.S. (1995). Decreased content of protein 4.2 in ankyrin-deficient normoblastosis (nb/nb) mouse red blood cells: evidence for ankyrin enhancement of protein 4.2 membrane binding. *Blood* 86, 3583–3589.
- Schoenheimer, R., and Rittenberg, D. (1935). Deuterium as an indicator in the study of intermediary metabolism. *Science* 82, 156–157.
- Schulze, W.X., and Mann, M. (2004). A novel proteomic screen for peptide-protein interactions. *J. Biol. Chem.* 279, 10756–10764.
- Shevchenko, A., Wilm, M., Vorm, O., and Mann, M. (1996). Mass spectrometric sequencing of proteins silver-stained polyacrylamide gels. *Anal. Chem.* 68, 850–858.
- Shi, Z.T., Afzal, V., Collier, B., Patel, D., Chasis, J.A., Parra, M., Lee, G., Paszty, C., Stevens, M., Walensky, L., et al. (1999). Protein 4.1R-deficient mice are viable but have erythroid membrane skeleton abnormalities. *J. Clin. Invest.* 103, 331–340.
- Southgate, C.D., Chishti, A.H., Mitchell, B., Yi, S.J., and Palek, J. (1996). Targeted disruption of the murine erythroid band 3 gene results in spherocytosis and severe haemolytic anaemia despite a normal membrane skeleton. *Nat. Genet.* 14, 227–230.
- Taouatas, N., Drugan, M.M., Heck, A.J., and Mohammed, S. (2008). Straightforward ladder sequencing of peptides using a Lys-N metalloendopeptidase. *Nat. Methods* 5, 405–407. Published online April 20, 2008. 10.1038/nmeth.1204.
- Ussar, S., Wang, H.V., Linder, S., Fassler, R., and Moser, M. (2006). The Kindlins: subcellular localization and expression during murine development. *Exp. Cell Res.* 312, 3142–3151.
- Wolfe, R.R., and Chinkes, D.L. (2005). *Isotope tracers in metabolic research* (New Jersey: Wiley-LISS).
- Wu, C.C., MacCoss, M.J., Howell, K.E., Matthews, D.E., and Yates, J.R., 3rd. (2004). Metabolic labeling of mammalian organisms with stable isotopes for quantitative proteomic analysis. *Anal. Chem.* 76, 4951–4959.
- Zhang, Y., Zhang, Y., Adachi, J., Olsen, J.V., Shi, R., de Souza, G., Pasini, E., Foster, L.J., Macek, B., Zougman, A., et al. (2007). MAPU: Max-Planck Unified database of organellar, cellular, tissue and body fluid proteomes. *Nucleic Acids Res.* 35, D771–D779.